PATH-DEPENDENT CYCLIC STRESS-STRAIN RELATIONSHIP OF REINFORCING BAR INCLUDING BUCKLING

Rajesh Prasad Dhakal [a,*], Koichi Maekawa [b]

[a] Protective Technology Research Centre, School of Civil and Environmental Engineering, Nanyang Technological University, 50 Nanyang Avenue, Singapore 639798.

[b] Department of Civil Engineering, The University of Tokyo, Hongo 7-3-1, Bunkyo-Ku, Tokyo 113-8656, Japan.

Abstract: In this paper, formulation and verification of a cyclic stress-strain relationship of reinforcing bars are presented. The tension envelope comprises an elastic range, a yield-plateau and a hardening zone. The compression envelope also includes a linear elastic range followed by a nonlinear buckling model. The cyclic loops follow Giuffre-Menegotto-Pinto equations with some modifications to account for the effect of buckling. A complete path-dependent cyclic constitutive model is then obtained by combining the equations representing the two monotonic envelopes and the cyclic loops. Comparison with bare bar test results showed that the proposed model could reasonably predict the cyclic behaviour of reinforcing bars including the post-buckling loops.

Key words: buckling; reinforcing bar; envelope; cyclic loop; path-dependent; stress-strain relationship

1. Introduction

As performance based design method is gaining popularity, reliable assessment of seismic performance has emerged as a vital step in seismic design. With the advancement in computing facilities that can easily handle complicated and large-scale mathematical operations, computational models with wider scope and greater accuracy are being developed regardless of their complexity. Although analysis based on member/component models can provide global structural behaviour, constitutive models of constituent material are needed to evaluate local response and also to assess damage. An important constituent of reinforced concrete (RC) members is reinforcement, which has dominant contribution in the overall seismic response. Reinforcing bars inside RC structures experience wide range of strain variations when subjected to a seismic excitation. Apart from experiencing large tensile and compressive strains, these bars also undergo random strain reversals from different strain levels. As the post-elastic response of reinforcing bars depends on strain history, a reliable path-dependent cyclic stress-strain relationship that can cover all possible strain paths is deemed necessary for evaluating structural seismic performance analytically.

Some cyclic constitutive models for reinforcing bars have been proposed recently. However, many of them do not incorporate the effect of buckling [1-3]. Hence, these models are applicable either to thick bars that are unlikely to buckle within reasonable compressive strain range or to loading cases where strain does not reach high in compression. As buckling of reinforcing bars in RC members is not uncommon during seismic excitations, proper consideration of buckling is necessary for seismic performance evaluation, and models which ignore buckling are hence not ideal to be used in seismic analysis of RC structures. Buckling induced instability of reinforcing bars inside RC members has been extensively studied in the past [4-9]. Some of these studies also discussed average compressive response of reinforcing bars including buckling, but none came up with a complete cyclic model. The authors are aware of a few cyclic models [10-12] that are reported to include the effect of buckling.

Rodriguez et al. [12] conducted monotonic and cyclic tests on deformed steel bars. Based on test results of several specimens, they proposed equations to locate *onset of buckling* during monotonic and cyclic loadings. They also proposed a cyclic constitutive model, which is basically the same as that proposed by Mander et al. [1] for cases without buckling with an additional recommendation to curtail the model at the *onset of buckling*. Nevertheless, this model is silent on the post-buckling response of reinforcing bars. Direct measurement of steel stress inside RC columns [10] and cyclic tests on bare bars [11] have shown that reinforcing bars can carry significant tensile stress even after the initiation of buckling, although the compressive stress carrying capacity decreases. One of the most informative studies on reinforcement buckling is conducted by Suda et al. [10], in which they monitored the stress carried by reinforcing bar inside RC columns with a specially designed stress sensor. With the help of these special test results and some assumptions, they came up with a cyclic stress-strain relationship of reinforcing bars including buckling. However, this relationship suggests a common post-buckling behaviour for all bars regardless of their geometrical and mechanical properties. This does not seem logical, as past studies [6,7,13] have shown that the buckling initiation point and the post-buckling response is sensitive to the bar length to bar diameter ratio (i.e. the slenderness ratio) and yield strength of the bar. In another genuine effort, Monti and Nuti [11] conducted monotonic and cyclic tests on some normal strength deformed steel bars, and concluded that buckling takes place only in bars with slenderness ratio greater than 5. Based on the test results, they proposed equations to relate average compressive

[*]Corresponding author, Tel: +65-6790-4150; Fax: +65-6791-0046; E-mail: cdhakal@ntu.edu.sg

response with the slenderness ratio. They also theoretically derived equations for cyclic loops based on different hardening rules for cases with and without buckling, and modified an existing cyclic model [14] to represent results of the tests that included buckling. However, the equations proposed and the constants included were derived to fit the test results of normal strength bars (f_y = 480 MPa) with slenderness ratio equal to 5, 8 and 11 only. Consequently, these equations cannot be general as they cover only a narrow range of geometrical properties and do not take into account the effect of yield strength and bar types.

This paper presents a path-dependent cyclic model for reinforcing bars that overcomes the aforementioned shortcomings. The model proposed here fulfils the following requirements: 1) It takes into account the effect of geometrical and mechanical properties of bar in its post-buckling response, and is applicable to bars with any material properties and any type of hardening mechanism. 2) It is of $\sigma = f(\varepsilon)$ type, which offers significant advantages in any nonlinear finite element computation based on kinematic approximations, as in displacement controlled FEM analysis. 3) It is fully path-dependent and covers all possible strain paths. 4) It is simple in formulation and is based on material parameters that are readily available, making it easy to implement/encode into any FEM analysis programs.

2. Uniaxial Monotonic Curves

Manufacturers of reinforcing bars usually provide mechanical properties that partly or completely define the uniaxial tensile behaviour of their products. Nevertheless, values of these parameters in compression are seldom specified, thus implicitly compelling to assume that these properties are isotropic and are equal in tension and compression. It is true when we talk about the point wise stress-strain relationships because the point wise relationships are not influenced by the change in overall geometry [2]. On the other hand, average tensile and compressive behaviours are not necessarily the same, as a geometrical nonlinearity exists in compression [13] due to lateral deformation of reinforcing bars; referred to as buckling hereafter. As monotonic compression test results [1,11] suggest that the average compressive stress-strain curves of reinforcing bar samples with slenderness ratio small enough to avoid premature buckling are very close to the corresponding tension envelopes, it is assumed in this study that the average compressive and tensile envelopes are similar in absence of buckling.

2.1 Tension envelope

Accurate representation of tension envelope becomes indispensable to ensure the accuracy of the complete cyclic model because both compression envelope and cyclic loops are influenced by the tension envelope. Note that specifying only yield strength, Young modulus and breaking strength does not completely describe the tensile response of a bar. To trace the post-yielding tensile response until breaking, it is necessary to specify the range of yield-plateau, nature of strain-hardening, hardening stiffness, and breaking strain. The authors are of the view that it is not appropriate to extrapolate the hardening behaviour of a bar based on its elastic properties. Tensile properties of deformed bars reported in references [8,11,15,16] manifest that hardening behaviours of bars with different yield strength and manufactured in different parts of the globe are significantly different from each other. As the hardening behaviour of deformed bars becomes more brittle with increase in yield strength, normalizing the post-yield tension parameters with respect to the yield stress and yield strain cannot be justified. In order to generate a universal cyclic model that can be used for bars with any type of hardening behaviour, the complete tension envelope is used as an input.

Regardless of the manufacturer and yield strength, tension envelop of all bars can be qualitatively represented as shown in Fig. 1(a). The tension envelope consists of four parts: elastic branch (O-Y), yield-plateau (Y-H), strain-hardening zone (H-U), and the post-ultimate descending branch (U-F). Although a closer look inside the yield-plateau is reported to exhibit small stress undulations [2], it is represented here as a straight line with the stress equal to yield strength for simplicity. As the final post-ultimate descending branch is of less significance in RC structural analysis, tension envelope only up to the ultimate stress point is usually considered. Tension envelop until the strain-hardening point ε_{sh} can be represented by the following uniaxial stress-strain (σ_{st} - ε_{st}) relationships.

$$\sigma_{st} = E_s \varepsilon_{st} \qquad \text{for } \varepsilon_{st} \le \varepsilon_y \tag{1}$$

$$\sigma_{st} = f_y \qquad \text{for } \varepsilon_y < \varepsilon_{st} \le \varepsilon_{sh} \tag{2}$$

In equations (1) and (2), E_s, f_y, ε_y and ε_{sh} are Young modulus, yield strength, yield strain, and strain at the starting point of hardening, respectively. Mander et al. [1] proposed the following equations to idealize the nonlinear strain-hardening branch.

$$\sigma_{st} = f_u + (f_y - f_u)\left(\frac{\varepsilon_u - \varepsilon_{st}}{\varepsilon_u - \varepsilon_{sh}}\right)^P \qquad \text{for } \varepsilon_{sh} < \varepsilon_{st} \le \varepsilon_u \tag{3}$$

$$P = E_{sh}\left(\frac{\varepsilon_u - \varepsilon_{sh}}{f_u - f_y}\right) \tag{4}$$

Here, f_u and ε_u are respectively the stress and strain at the ultimate point, and P is a parameter that describes the shape of hardening curve. P can be calculated as shown in equation (4), where E_{sh} is the tangential stiffness of the hardening curve at the starting point. Note that P equal to zero (i.e. $E_{sh} = 0$) represents an elasto-plastic bar, and P equal to 1 (i.e. $E_{sh} = (f_u - f_y)/(\varepsilon_u - \varepsilon_{sh})$) represents a bar with linear strain hardening behaviour. Although coordinates of the strain-hardening point and the ultimate point can be located in an envelope, it is not easy to correctly measure E_{sh}. To avoid the uncertainty involved in estimating E_{sh}, Rodriguez et al. [12] proposed the following equation that utilizes the coordinates of any point (ε_{sh1}, f_{sh1}) in the strain-hardening zone to evaluate P.

$$P = \frac{\log\left(\frac{f_u - f_{sh1}}{f_u - f_y}\right)}{\log\left(\frac{\varepsilon_u - \varepsilon_{sh1}}{\varepsilon_u - \varepsilon_{sh}}\right)} \tag{5}$$

If the correct value of initial hardening stiffness E_{sh} is not known, the authors also prefer to use equation (5) as it provides better control over the shape of strain-hardening curve. If an intermediate point is selected properly, a bilinear approximation as shown in Fig. 1(b) can also closely represent the hardening curve. However, the selection of the intermediate point (ε_{sh1}, f_{sh1}) is difficult, when only the extreme points of strain-hardening curve are supplied and the nature of the hardening curve in between is not known. In such cases, it is recommended to assume $\varepsilon_{sh1} = [0.5(\varepsilon_{sh} + \varepsilon_u)]$, and $f_{sh1} = [f_y + 0.75(f_u - f_y)]$.

2.2 Compression envelope

As mentioned earlier, the average compressive response within a control volume including the effect of buckling is different from the tensile one, although the point wise stress-strain relationships in tension and compression are the same regardless of buckling. In the past, a few average compressive stress-strain relationships including buckling have been proposed [11,12] to satisfy the results of the tests, which were conducted within a small range of slenderness ratio. Because of different material properties used in these tests, the empirical relationships derived differ considerably with each other. Although the equations proposed could predict the effect of slenderness ratio in the tested range, they do not account for the effect of other parameters such as yield strength that was not varied in the tests. As a general model has to cover conditions that are hardly reproduced in the tests, the experiments planned for obtaining widely applicable constitutive models should consist of test specimens that systematically cover wide range of geometrical as well as mechanical properties. Experiments consisting of a few specimens with random properties are, of course, informative, and better suited to verify proposed models rather than to generate new models based on them.

In order to generate data for model formulation, the authors conducted an analytical parametric study based on fibre technique [14], where the elements were intentionally chosen to be of small length to ensure that the behaviour within an element is unaffected by global geometrical alterations. Hence, the use of tension envelope to represent compressive stress-strain relationship of the fibres in each element regardless of the extent of buckling is justified. To reproduce actual test condition, rotation and displacement at the two extreme nodes were restrained, and an axial downward displacement was gradually applied at the topmost node. Of course, the analytical tool was experimentally verified [13] before conducting the extensive parametric study. Length L, diameter D and yield strength f_y of the bar were identified to govern the axial load-displacement relationship, and these three parameters were varied within wide ranges to investigate their effect on the average compressive response.

Detailed discussions on the analytical method and the results are out of scope of this paper, and have been reported in another paper [13]. A typical result of the parametric study for elastic perfectly plastic bar is illustrated in Fig. 2. The comparative normalized average stress-strain curves for slenderness ratios 5 and 10 and yield strengths

ranging from 100 MPa to 1600 MPa are presented in Figs. 2(a) and (b) respectively. The results suggest that the critical slenderness ratio below which the effect of buckling is negligible depends also on yield strength of the reinforcing bar. Interestingly, two pairs of special cases [i) f_y = 100 MPa, L/D = 10 and f_y = 400 MPa, L/D = 5; and ii) f_y = 400 MPa, L/D = 10 and f_y = 1600 MPa, L/D = 5] compared in Fig. 2(c) showed similar average responses for the two cases in each pair, suggesting that the normalized average compressive response depends only on $L/D\sqrt{f_y}$. The variation of normalized compressive stress with $L/D\sqrt{f_y}$ is shown in Fig. 2(d). As the value of $L/D\sqrt{f_y}$ increases, the buckling-induced stress degradation becomes severer. Next, similar parametric study is conducted for reinforcing bars with a linear strain-hardening behaviour as shown in Fig. 3(a). The normalized compressive stress-strain curves for these bars with slenderness ratios ranging from 5 to 15 for yield strengths equal to 200, 400 and 800 MPa are shown in Figs. 3(b)-(d), respectively. In this case too, the average compressive response was found to uniquely depend on $L/D\sqrt{f_y}$, irrespective of separate values of L, D and f_y. The past studies could not unearth this unique interrelationship, which is the backbone of the model proposed in this paper.

Through this analytical parametric study, various facts regarding the average behaviour of reinforcing bars in compression are revealed. Some of them are: 1) The average compressive stress-strain relationship can be completely described by $L/D\sqrt{f_y}$. 2) The average compression envelope lies below the tension envelope when plotted together. 3) The trend of average compressive stress degradation depends on the value of $L/D\sqrt{f_y}$ and also on the tension envelope. 4) Regardless of $L/D\sqrt{f_y}$, the compressive stress degradation rate in the later stage is nearly constant with a negative slope approximately equal to $0.02E_s$. 5) The average compressive stress becomes constant after it becomes equal to 20% of the yield strength. Guided by these unique interrelationships, an average monotonic compressive stress-strain relationship is proposed, the general layout of which is sketched in Fig. 4. Note that the compressive stresses and strains specified in Fig. 4 and used in the equations to follow are absolute, and their signs should be changed before merging with the tension envelope and unloading/reloading loops to form a complete cyclic model. An intermediate point (ε_i, f_i) is established, after which a constant negative stiffness equal to $0.02E_s$ is applied until the average compressive stress becomes equal to $0.2f_y$. To represent the aforementioned mechanisms, following compressive stress-strain (σ_{sc}-ε_{sc}) relationships are proposed.

$$\sigma_{sc} = E_s \varepsilon_{sc} \qquad \text{for } \varepsilon_{sc} \le \varepsilon_y \tag{6}$$

$$\frac{\sigma_{sc}}{\sigma_t} = 1 - \left(1 - \frac{f_i}{f_{it}}\right)\left(\frac{\varepsilon_{sc} - \varepsilon_y}{\varepsilon_i - \varepsilon_y}\right) \qquad \text{for } \varepsilon_y < \varepsilon_{sc} \le \varepsilon_i \tag{7}$$

$$\sigma_{sc} = f_i - 0.02E_s(\varepsilon_{sc} - \varepsilon_i); \qquad \sigma_{sc} \ge 0.2f_y \qquad \text{for } \varepsilon_{sc} > \varepsilon_i \tag{8}$$

Here, σ_t and f_{it} are stresses in the tension envelope corresponding to ε_{sc} (current strain) and ε_i (strain at the intermediate point), respectively. To make the model applicable to bars with all types of material model, the compressive stress σ_{sc} at and before the intermediate point is normalized with respect to σ_t. This normalization technique also renders the shape of the average compression envelope before this intermediate point look like the tension envelope; a characteristic that was distinctly observed in all analytical results. The coordinates of intermediate points in the analytically generated average compression envelopes could be correlated to $L/D\sqrt{f_y}$ as:

$$\frac{\varepsilon_i}{\varepsilon_y} = 55 - 2.3\sqrt{\frac{f_y}{100}}\frac{L}{D}; \qquad \frac{\varepsilon_i}{\varepsilon_y} \ge 7 \tag{9}$$

$$\frac{f_i}{f_{it}} = \alpha\left(1.1 - 0.016\sqrt{\frac{f_y}{100}}\frac{L}{D}\right); \qquad \frac{f_i}{f_y} \ge 0.2 \tag{10}$$

Comparison between the average compression envelopes of the elastic perfectly plastic and the linear strain-hardening bars revealed that the normalized strain at the intermediate point ($\varepsilon_i/\varepsilon_y$) was almost unaffected but the normalized stress (f_i/f_{it}) was sensitive to the nature of strain hardening. To account for this effect, a coefficient α is included in the formulation of stress at the intermediate point in equation (10). The value of α is found to be 0.75 for elastic perfectly plastic bars, and 1.0 for bars with continuous linear hardening. For bars with limited hardening

range, in which most of the industrial products fall, it should be chosen between 0.75 and 1. If the hardening stiffness is very small or the hardening range in terms of strain is short, α should be closer to 0.75. On the other hand, if the hardening lasts for large strain range, it should be closer to 1.0. To represent this qualitative interrelationship, the following equations are recommended to compute α.

$$\alpha = 0.75 + \frac{\varepsilon_u - \varepsilon_{sh}}{300\varepsilon_y}; \qquad \alpha \le \frac{f_u}{1.5 f_y}; \qquad 0.75 \le \alpha \le 1.0 \tag{11}$$

2.3 Verification of the proposed average compression envelope

For verification of the proposed compression envelope, monotonic compression test results of Monti and Nuti [11] are used. These tests were performed on medium-strength steel reinforcing bars with different slenderness ratios (5, 8 and 11), and three different bar diameters of 16 mm, 20 mm and 24 mm were used for each slenderness ratio. As it was reported that the behaviour of the shortest bar almost coincides with the material model, the tension envelope was fairly assumed to match the average response of the bar with slenderness ratio 5, which yielded the following: E_s = 200 GPa; f_y = 480 MPa; ε_y = 0.0024; $\varepsilon_{sh} = \varepsilon_y$; $\varepsilon_u = 16\varepsilon_{sh}$; $f_u = 1.4f_y$; E_{sh1} (between ε_{sh} and $6\varepsilon_{sh}$) = $0.055E_s$; E_{sh2} (between $6\varepsilon_{sh}$ and $11\varepsilon_{sh}$) = $0.025E_s$; E_{sh3} (between $11\varepsilon_{sh}$ and $16\varepsilon_{sh}$) = 0. The normalized average stress-strain curves obtained using the proposed average compression envelope and measured in the tests are compared in Fig. 5(a). The model predictions are in fair agreement with the experimental results for all three cases of monotonic loading. However, small difference can be observed because the assumed material properties may not have correctly represented the actual tension envelope.

To check the applicability of the proposed envelope for different range of yield strength, results of the tests conducted by Mander et al. [1] are used next. As the tension and compression envelopes of the tested bars are well documented [6], the scope of uncertainties is also eliminated. As reported, compression envelope of the tested bars without buckling was represented by the following: E_s = 200 GPa; f_y = 290 MPa; ε_y = 0.00145; $\varepsilon_{sh} = 11.7\varepsilon_y$; f_u = 433 MPa; ε_u = 0.1; E_{sh} = 4400 MPa. The experiment consists of direct compression tests of five low-strength reinforcing bars with different slenderness ratios (5.5, 6, 6.5, 10 and 15). The comparison is shown for only three cases as the results of the first three specimens are found to be very close to each other, and only one representative case (L/D = 6) among these three was chosen. The normalized average stress-strain curves obtained from the test are compared with the proposed average compression envelopes in Fig. 5(b). The two curves are both qualitatively and quantitatively in good agreement with each other giving ample proof of the reliability of the proposed envelope.

2.4 Improvement over the existing compression models

The authors' are aware of only one model [11] that explicitly includes equations to represent average compressive stress-strain relationship including buckling. In this model proposed by Monti and Nuti [11], the plastic strain range ($\gamma_s = \varepsilon_{5\%} - \varepsilon_y$) within which the difference between the average compressive stress and the tensile stress is less than 5% can be expressed as:

$$\gamma_s = \frac{11 - \frac{L}{D}}{e^{c(L/D)} - 1} \ge 0; \qquad \text{for } 5 < \frac{L}{D} \le 11 \tag{12}$$

In equation (12), L/D is the slenderness ratio and *c* is an experimental constant equal to 0.5 for the bars tested by Monti and Nuti [11]. Similarly, the softening stiffness b^- after yielding is expressed as shown in equation (13), where $(L/D)_{cr}$ is the critical slenderness ratio below which the compression monotonic curve essentially coincides with the tensile curve, and *a* is an experimental constant. The reported value of $(L/D)_{cr}$ is 5, and that of the constant *a* corresponding to the secant slope ratio (from ε_y to $\varepsilon = 10\varepsilon_y$) is 0.006. Moreover, the softening branch is modelled to converge asymptotically to a value σ_∞ given by equation (14), where f_y is the yield strength of the reinforcing bar.

$$b^- = a\left[\left(\frac{L}{D}\right)_{cr} - \frac{L}{D}\right]; \qquad \text{for } \frac{L}{D} > \left(\frac{L}{D}\right)_{cr} \tag{13}$$

$$\sigma_{\infty} = \frac{6 f_y}{L/D}; \tag{14}$$

Although these equations yield good correlation with the test results with slenderness ratio 5 and 11, the case with slenderness ratio equal to 8 cannot be predicted due primarily to a large value of γ_s given by equation (12). In fact, equation (12) significantly overestimates the value of γ_s for all values of L/D ratio less than 11, forcing the authors to suspect that there must have been a typographical error. Once the slenderness ratio is equal to or greater than 11, the compression curve is independent of equation (12) and the other two equations govern the average compressive stress-strain relationship. Hence, Mander et al's [1] monotonic compression test results of a reinforcing bar with slenderness ratio 15 is chosen here for the comparison of the proposed model with Monti and Nuti's model. Comparison of these two models with the test result and the tension envelope is shown in Fig. 6. Monti and Nuti's model predicts steeper softening in small strain region and restricts the minimum compressive stress to $0.4f_y$. In contrast, test result shows a sustained softening of average compressive stress throughout the applied strain range. As the effect of bar strength was not taken into account and the model was developed based on the test results of medium strength bars only, the prediction of Monti and Nuti's model is far from the actual average behaviour of a bar with lower yield strength. On the other hand, the proposed model closely follows the experimental curve throughout the applied strain range, showing significant improvement over Monti and Nuti's model.

3. Uniaxial Cyclic Loops

Although tension and compression envelopes are enough to cover monotonic loading that is usually followed in laboratory tests, they cannot handle load reversal that is an integral part of seismic loading. Cyclic models are pre-requisite to reproduce hysteresis loops that define energy dissipation capacity, which is an important parameter in seismic performance evaluation of RC structures. In the past, a few models representing cyclic stress-strain relationships have been proposed, and verified with test results that did not include buckling [3,14,15,17]. All of these models proposed equation to represent a nonlinear transition from the strain-reversal point to the maximum strain in the opposite direction that was ever reached before. However, some of them did not include provision to control the approaching stiffness at the target point. This is acceptable if buckling is neglected, because tangential stiffness in an average compression envelope without buckling, which is similar to the tension envelope, always varies between zero and a small positive value. Hence, a constant representative stiffness would satisfactorily represent all cases if buckling is overlooked. Nevertheless, tangential stiffness of compression envelope that includes buckling may not always be positive, and the possible negative stiffness varies widely depending on the geometrical and mechanical properties of the bar. A negative stiffness at the minimum strain point may generate an unloading curve that shows compressive stress reduction even before entering the compressive strain zone. This tendency in the cyclic loops can be simulated only if the stiffness at the target point is also taken into account in formulating the trajectory of the loop. Therefore, Giuffre-Menegotto-Pinto model [18] that satisfies the aforementioned condition is adopted in this study, and some modifications are made to account for the effects of buckling.

3.1 Original Giuffre-Menegotto-Pinto model

As illustrated in Fig. 7, Giuffre-Menegotto-Pinto model [18] uses a smooth transition curve asymptotic to the tangents at the strain reversal point; i.e. the origin, and the maximum strain in the opposite direction ever achieved; i.e. the target point. The original model can be expressed in the form of normalized stress-strain relationship as in the following equations:

$$\sigma_{eq} = b\varepsilon_{eq} + \frac{(1-b)\varepsilon_{eq}}{\left(1+\varepsilon_{eq}^{R}\right)^{1/R}} \tag{15}$$

$$\varepsilon_{eq} = \frac{\varepsilon_s - \varepsilon_r}{\varepsilon_0 - \varepsilon_r}; \qquad \sigma_{eq} = \frac{\sigma_s - \sigma_r}{\sigma_0 - \sigma_r} \tag{16}$$

$$R = R_0 - \frac{a_1 \xi}{a_2 + \xi} \tag{17}$$

In equation (15), b is strain-hardening ratio defined by the ratio between the intended slope at the target point and the unloading/reloading stiffness at the origin. The normalized strain ε_{eq} and the normalized stress σ_{eq} can be calculated according to equation (16), where $(\varepsilon_0, \sigma_0)$ is the intersection (point I in Fig. 7) of the two tangents ((a) and (b) in Fig. 7), and $(\varepsilon_r, \sigma_r)$ is the origin (point A in Fig. 7). Similarly, R is a parameter that influences the shape of the transition curve, and is expressed as shown in (17). Here, ξ is the strain difference between the tangents intersection point and the target point (point B in Fig. 7) normalized with respect to the yield strain. R_0 is the value of parameter R during the first loading, and should be experimentally defined along with constants a_1 and a_2. These equations represent a smooth transition from the unloading/reloading stiffness at the origin to the intended approaching stiffness at the target point. Note that the target point always lies in an envelope although the origin can be inside a loop itself. As the maximum and minimum strain points are target points for potential cyclic loops, the stiffness at these extreme points is also stored in the memory in addition to their coordinates. These values are updated once the strain goes outside the range defined by the positive and negative maximum strains. To ensure path-dependency, a new tangent intersection point is established and the value of R is computed for each new strain reversal.

3.2 Experimental constants

To know the values of the experimental constants R_0, a_1 and a_2 for a reinforcing bar, cyclic test on some samples are needed. The users would be relieved of this inconvenience, if values of these constants that are applicable to most bar types were known beforehand. A parametric investigation targeted to study the influence of these constants on the overall cyclic loop revealed that with the increase in the positive value of R, the loop becomes closer to the bilinear transition formed by the tangents at the origin and the target points. Provided that the resulting value of R is positive, the transition becomes smoother if the value of a_1 increases or that of R_0 and/or a_2 decreases. However, making the transition smoother will increase the difference between the stress of the target point and the stress at the same strain in the cyclic loop, termed as stress-shift hereafter. While assigning the values to these constants, one should hence be careful not to induce an unreasonably large stress-shift, and should also ensure that the value of R remains positive. As these constants do not influence the monotonic curve and small changes in their values affect the transition shapes only marginally, the authors after extensive checking found that $R_0 = 20$; $a_1 = 18.5$; and $a_2 = 0.15$ yield reasonable curves.

3.3 Stiffness at the target and the origin

As mentioned earlier, the stiffness intended at the target point and the unloading or reloading stiffness at the origin are needed to compute the strain-hardening ratio b. For a reloading loop as shown in Fig. 7, the target point is the maximum tensile strain point, and the target stiffness is equal to the hardening stiffness at the maximum strain point stored in the memory. For an unloading loop, the tangential stiffness at the target point (maximum compressive strain ever reached) can be positive or negative depending on the extent of buckling occurred before. The target stiffness, if positive, is always smaller than the tangential stiffness of the tension envelope at an equal tensile strain. On the other hand, depending on the value of the parameter $L/D\sqrt{f_y}$, the negative tangential stiffness varies widely. Using a large negative value for the target stiffness is likely to generate unloading loops that show unreasonably large compressive stress near the tangent intersection point. To avoid this undesirable circumstance, the negative slope of a line joining the minimum strain point to the yielding point in compression as shown in Fig. 8 is used as the target stiffness, which is again not allowed to exceed 3% of the Young's modulus.

Test results [10,11] have shown that reloading stiffness from the post-buckling compression state is significantly smaller than the Young's modulus E_s. This is due primarily to the gradual loss of axial stiffness in the post-buckling stage. The stiffness of a buckled bar comes mainly from flexure, and the axial stiffness fully participates only after the bar is straightened [11]. As shown in Fig. 9, the reloading stiffness from a compression envelope is almost equal to the Young's modulus if tension envelope is used to represent the compression envelope. The larger the buckling-induced compressive stress reduction at the reloading point, the less the reloading stiffness would be. To qualitatively account for this interrelationship, the reduced reloading stiffness E_b from compression envelope is derived as:

$$E_b = E_s \left(\frac{\sigma_{\min}}{\sigma_{t\min}} \right)^2; \qquad E_b \le E_s \qquad \text{for } \varepsilon_r < -\varepsilon_y \tag{18}$$

In equation (18), σ_{min} and σ_{tmin} are stresses at the minimum strain point in the compression envelope and the tension envelope plotted in the compression side, respectively. Note that the amendments suggested above come into existence only in occurrence of buckling, and necessarily yield similar results as the original Giuffre-Menegotto-

Pinto model if buckling-induced compressive stress degradation has not taken place. For a strain reversal from the post-yield region in tension envelope, the unloading stiffness E_u is reported to reduce with increase in the maximum plastic tensile strain [19]. Following the equation by Dodd and Restrepo-Posada [2], the interrelationship between the unloading stiffness E_u normalized with respect to the Young's modulus E_s and the maximum plastic tensile strain ε_m is expressed as:

$$\frac{E_u}{E_s} = 0.82 + \frac{1}{5.55 + 1000\varepsilon_m} \tag{19}$$

It is reported [2] that the unloading stiffness shows a small recovery for reversals that occur before reaching the target point. The unloading stiffness is hence assumed to vary only with the maximum plastic strain regardless of the unloading point, and equation (19) is used for all unloading loops. Similarly, the reloading stiffness E_b computed by equation (18) is also, for convenience, used for all reloading loops regardless of the reloading point. To facilitate the path-dependent computation, the unloading stiffness E_u is updated once the maximum tensile strain is exceeded and the reloading stiffness E_b is updated once the maximum compressive strain is exceeded.

3.4 Merging cyclic loop with the envelopes

The modified Giuffre-Menegotto-Pinto model is combined with the aforementioned tension and compression envelopes to formulate a general path-dependent cyclic stress-strain relationship for reinforcing bars. Note that the cyclic loops describe the response until the previously attained maximum/minimum strain point (i.e. the target point) only, and response to further continuous loading in the same direction follows the corresponding envelope. As mentioned earlier, the stress at target point is less in the cyclic loops than in the corresponding envelope; i.e. a stress-shift exists at the target strain. Fig. 9 explains a method adopted to avoid a sudden jump due to this stress-shift at the target strain, which might create convergence problem during FEM iterations. When a loop completes and the loading is continued further in the same direction, a linearly reducing fraction of this stress-shift is deducted from the envelope stress until the difference is completely nullified at $5\varepsilon_y$ ahead of the target point. If another loop starts before the stress-shift is nullified, the residual stress-shift at the strain reversal point is stored in the memory. As shown in Fig. 9, half of the residual stress-shift is deducted from the corresponding envelope stress to obtain target stress for the next loop in the same direction.

4. Verification of the Proposed Cyclic Model

As the proposed cyclic model is different from existing models only in the occurrence of buckling, its performance is necessarily similar to that of other models if the strain history does not cover significant compressive strain to cause buckling. Plenty of experimental verifications can be found in references [1,12,18], where the stress-strain curves predicted by the corresponding cyclic models are proved to be close to the cyclic test results that did not include buckling. It is hence necessary to verify the proposed model only for cyclic loading cases that include buckling. For this purpose, cyclic test results of Monti and Nuti [11] are adopted because these are the only cyclic tests known to the authors, where the loading history comprises strain reversals from the post-buckling stage.

Material properties of the specimens in all eight tests considered here and the strain history followed in each of these tests are listed in Table 1. The three S-series tests refer to symmetrical cyclic loading of specimens with the same material properties but with different slenderness ratios, as indicated by the digit in their names. Similarly, the five C-series tests refer to unsymmetrical loading tests of specimens with slightly different material properties but with a constant slenderness ratio equal to 11, large enough to ensure that the specimens buckled. As the compression envelope has been verified earlier for different combinations of slenderness ratio and yield strength, verification of the path-dependency of the proposed cyclic model is performed here for a typical bar subjected to different loading paths including buckling. To highlight the importance of buckling, the experimental stress-strain curves are first compared with a cyclic model that uses the tension envelope to represent the compression behaviour (i.e. overlooks the effect of buckling) in Fig. 11. As buckling is difficult to occur in the shortest bar with slenderness ratio 5, the prediction is closer to the experimental curve. However in other cases with slenderness ratio equal to 8 and 11, the predicted curves are far from the test results, especially the compressive stress is significantly overestimated and the unloading paths are not accurately captured.

Next, the average cyclic responses observed in the experiment are compared with those obtained using the proposed model in Fig. 12. Basically, curves predicted by the proposed model are fairly close to the experimental results for all symmetric and non-symmetric loading tests, giving ample evidence of the reliability of the proposed path-dependent cyclic model. Paths of the unloading/reloading loops and the softening of compressive stress after

buckling observed in all arbitrary loading tests could be satisfactorily captured by the proposed model. Advocating the experimental facts, the model predictions also indicated that compressive stress does not soften for slenderness ratio 5, and the effect of buckling becomes more prominent for larger slenderness ratios. Tensile response was found to be independent of the extent of buckling achieved in previous cycles. Nevertheless, the proposed model could not predict stress deterioration due to the repeated cycles within a constant strain range, as observed in the experimental results of tests C3 and C4, and study to address this issue is being planned.

5. Application of the Proposed Model

The proposed path-dependent cyclic model is coupled with a cover concrete spalling criteria [20], and then modified for mesh-size consistency [21]. Next, this enhanced buckling model is installed in a 3-D finite element analysis program COM3 [22], which is used to conduct seismic analyses of a reinforced concrete (RC) column based on fibre technique. The column is discretized into several one-dimensional frame elements and the cross section is divided into many cells. In other words, each element consists of several parallel fibres including either concrete or reinforcing bars or a combination of both depending on the location of each fibre. The material models of concrete and reinforcing bars used in this analysis are fully path-dependent and are extensively verified [23] at material and member levels.

For experimental verification, a shake table test result of an eccentrically compressed RC column is adopted here [24]. Fig. 13 shows the geometrical details of the column, rebar details in the column cross-section, applied ground motion and the experimental as well as analytical results. To include the effect of inertia in the analysis, the axial compression force was replaced with an equivalent mass placed eccentrically at the column top. Time-history seismic analysis is conducted twice with and without using the enhanced buckling model. In the experiment, buckling of reinforcing bars and spalling of cover concrete were observed and a large residual displacement remained after the test. Although displacement larger than 13 cm could not be recorded in the test due to a technical problem with the transducer, the maximum and residual displacements are reported to be larger than 15 cm [24]. The analysis without incorporating the buckling model significantly underestimated the maximum and residual displacements, whereas the inclusion of the enhanced buckling model substantially improved the accuracy of the analytical prediction. The comparison of the experimental and analytical results indicates that the proposed buckling model can capture the buckling related mechanisms with reasonable accuracy. An extensive experimental verification of the buckling model at member level has been conducted [25] for RC and composite columns/piers subjected to pseudo-dynamic and seismic loadings.

6. Concluding Remarks

A complete path-dependent cyclic constitutive model for reinforcing bars is proposed. For the tension envelope, stress-strain equations describing the pre-yield elastic branch, constant-stress yield-plateau and nonlinear strain-hardening zone are presented. Thus defined tension envelope is used as an input to analytically generate average compression envelope. It was revealed that the average compression envelope of reinforcing bars including buckling depends only on the product of slenderness ratio (L/D) and the square root of yield strength ($\sqrt{f_y}$). To represent the average compressive stress-strain curves obtained through analysis, equations in the form of $\sigma = f(\varepsilon)$ with the tension envelope and $L/D\sqrt{f_y}$ as variables are formulated. Comparison with monotonic test results showed that the proposed equations are applicable for reinforcing bars with any geometrical and mechanical properties. For unloading and reloading loops, equations proposed by Giuffre-Menegotto-Pinto are supplemented with some additional equations to account for the effect of buckling on the unloading/reloading stiffness at the strain reversal point and also on the approaching stiffness at the target point. The equations describing monotonic curves and unloading/reloading loops are then combined to formulate a general path-dependent cyclic stress-strain relationship. Comparison with symmetric and asymmetric cyclic test results showed good agreement verifying the reliability of the proposed cyclic model. Although there are some rooms for improvement, this model in its current form offers significant improvement over the existing models, and can be readily used as the material model for reinforcing bars in FEM seismic analysis of RC members.

References

[1] Mander JB, Priestley MJN, Park R. Seismic design of bridge piers. Research Report 84-2. Department of Civil Engineering, University of Canterbury, Christchurch, New Zealand, 1984.

[2] Dodd LL, Restrepo-Posada JI. Model for predicting cyclic behavior of reinforcing steel. Journal of Structural Engineering, ASCE 1995;121:433-445.

[3] Balan TA, Filippou FC, Popov EP. Hysteretic model of ordinary and high-strength reinforcing steel. Journal of Structural Engineering, ASCE 1998;124:288-297.

[4] Scribner CF. Reinforcement buckling in reinforced concrete flexural members. ACI Journal 1986;83:966-973.

[5] Papia M, Russo G, Zingone G. Instability of longitudinal bars in RC columns. Journal of Structural Engineering, ASCE 1988;114:445-461.
[6] Mau ST, El-Mabsout M. Inelastic buckling of reinforcing bars. Journal of Engineering Mechanics, ASCE 1989;115:1-17.
[7] Mau ST. Effect of tie spacing on inelastic buckling of reinforcing bars. ACI Structural Journal 1990;87:671-678.
[8] Watson S, Zahn FA, Park R. Confining reinforcement for concrete columns. Journal of Structural Engineering, ASCE 1994;120:1798-1823.
[9] Pantazopoulou SJ. Detailing for reinforcement stability in RC members. Journal of Structural Engineering, ASCE 1998;124:623-632.
[10] Suda K, Murayama Y, Ichinomiya T, Shimbo H. Buckling behavior of longitudinal reinforcing bars in concrete column subjected to reverse lateral loading. Proceedings of the 11th World Conference on Earthquake Engineering 1996, CD ROM Paper No. 1753.
[11] Monti G, Nuti C. Nonlinear cyclic behavior of reinforcing bars including buckling. Journal of Structural Engineering, ASCE 1992;118:3268-3284.
[12] Rodriguez ME, Botero JC, Villa J. Cyclic stress-strain behavior of reinforcing steel including effect of buckling. Journal of Structural Engineering, ASCE 1999;125:605-612.
[13] Dhakal RP, Maekawa K. Modeling for post-yield buckling of reinforcement. Journal of Structural Engineering, ASCE (In Press).
[14] Menegotto M, Pinto PE. Method of analysis of cyclically loaded RC plane frames including changes in geometry and non-elastic behavior of elements under normal force and bending. Preliminary Report IABSE 1973;13:15-22.
[15] Kato B. Mechanical properties of steel under load cycles idealizing seismic actions. Bulletin D'Information No 131, AICAP-CEB Symposium on Structural Concrete Under Severe Seismic Actions, Rome 1979;7-27.
[16] Claeson C, Gylltoft K. Slender high-strength concrete columns subjected to eccentric loading. Journal of Structural Engineering, ASCE 1998;124:233-240.
[17] Aktan AE, Karlsson BI, Sozen MA. Stress-strain relationships of reinforcing bars subjected to large strain reversals. Civil Engineering Studies, Structural Research Series No.397, University of Illinois 1973.
[18] CEB. RC Elements under Cyclic Loading - State of the Art Report. Thomas Telford 1996.
[19] Bauschinger J. Variations in the elastic limit of iron and steel [summarized translation from "Mittheilungen aus dem Mechanischen Technischen Laboratorium der k. Hochschule in München]. Journal of Iron and Steel Institute 1887;1:442-444.
[20] Dhakal RP, Maekawa K. Reinforcement stability and fracture of cover concrete in RC members. Journal of Structural Engineering, ASCE (In Press).
[21] Dhakal RP, Maekawa K. Post-peak cyclic response analysis and energy dissipation capacity of RC columns. Journal of Materials, Concrete Structures, Pavements, JSCE 2001;51:117-133.
[22] Maekawa K. General information of COM3 (Concrete Model in 3-D) Version 9.5 – A user's manual. Department of Civil Engineering, The University of Tokyo 2000.
[23] Okamura H, Maekawa K. Nonlinear analysis and constitutive models for reinforced concrete. Gihodo Publication, Tokyo 1991.
[24] Kawashima K, Unjou S, Nagashima H, Iida H, Mukai H. An experimental study on seismic resistance and seismic performance of RC piers subjected to eccentric loading. Technical Memorandum of PWRI, Tsukuba 1995;3319.
[25] Dhakal RP, Maekawa K. Post-peak cyclic behavior and ductility of reinforced concrete columns. Modeling of Inelastic Behavior of RC Structures under Seismic Loads, ASCE 2001:193-216.

List of Figures:

Table 1. Material properties of specimens and strain history followed in each test

Test	f_y, MPa	E_s, GPa	ε_{sh}, %	ε_{sh1}, %	f_{sh1}, MPa	L/D	Strain history, %
S5	500	200	0.7	2	630	5	+1 –1 +2 –2 +3 -3
S8	500	200	0.7	2	630	8	+1 –1 +2 –2 +3 -3
S11	500	200	0.7	2	630	11	+1 –1 +2 –2 +3 -3
C1	470	200	0.7	4	660	11	+0.5 -0.5 +2.5 –1 +2 +0.4 +4 +1 +3 +1.5 +4
C2	470	200	0.7	4	660	11	+1 0 +1.5 -0.5 +2 -0.5 +4 +1.5 +3 +0.5 +4
C3	430	180	0.7	4	525	11	3(+1 –1) 2(+2 –1) 4(+2 –2)
C4	450	160	1.0	3	600	11	2(+3 –1) 2(+2 –1) 4(+3 –1)
C5	430	160	1.0	4	580	11	+1 –1 +2 –1 +3 –1 +4 -3

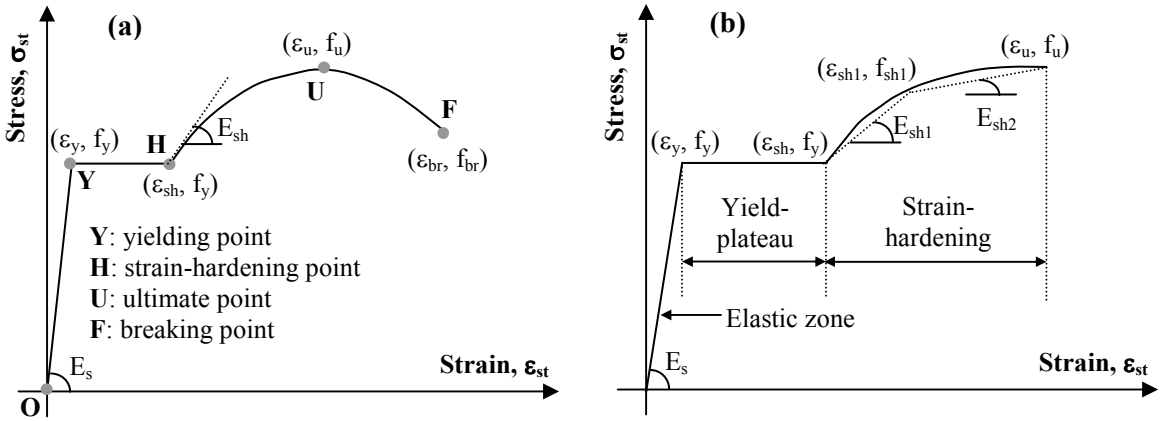
(a)
Stress, σst
(εu, fu)
U
F
(εy, fy)
H
Esh
(εbr, fbr)
Y
(εsh, fy)
Y: yielding point
H: strain-hardening point
U: ultimate point
F: breaking point
Es
Strain, εst
O
(b)
Stress, σst
(εsh1, fsh1)
(εu, fu)
Esh2
(εy, fy)
(εsh, fy)
Esh1
Yield-plateau
Strain-hardening
Elastic zone
Es
Strain, εst

Fig. 1

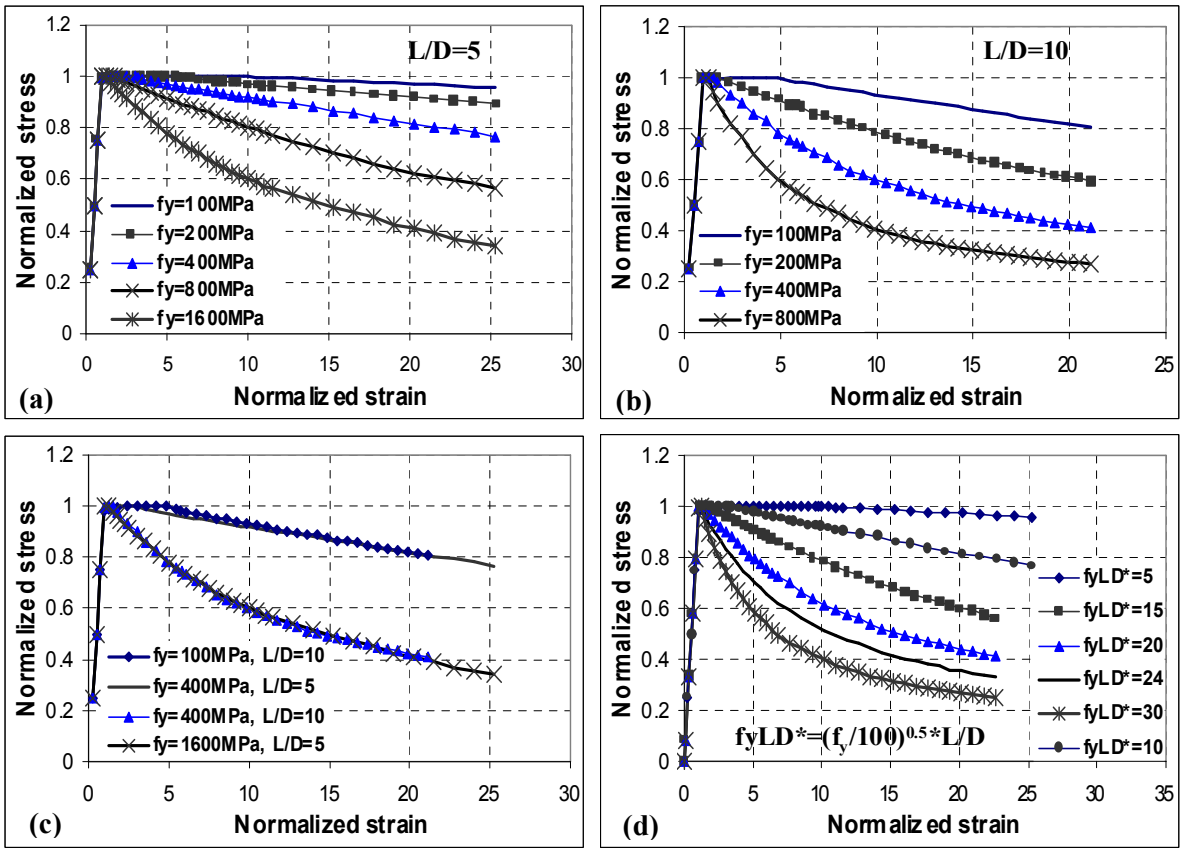
L/D=5
Normalized stress
Normalized strain
fy=100MPa
fy=200MPa
fy=400MPa
fy=800MPa
fy=1600MPa
(a)
L/D=10
Normalized stress
Normalized strain
fy=100MPa
fy=200MPa
fy=400MPa
fy=800MPa
(b)
Normalized stress
Normalized strain
fy=100MPa, L/D=10
fy=400MPa, L/D=5
fy=400MPa, L/D=10
fy=1600MPa, L/D=5
(c)
Normalized stress
Normalized strain
fyLD*=(fy/100)0.5*L/D
fyLD*=5
fyLD*=15
fyLD*=20
fyLD*=24
fyLD*=30
fyLD*=10
(d)

Fig. 2

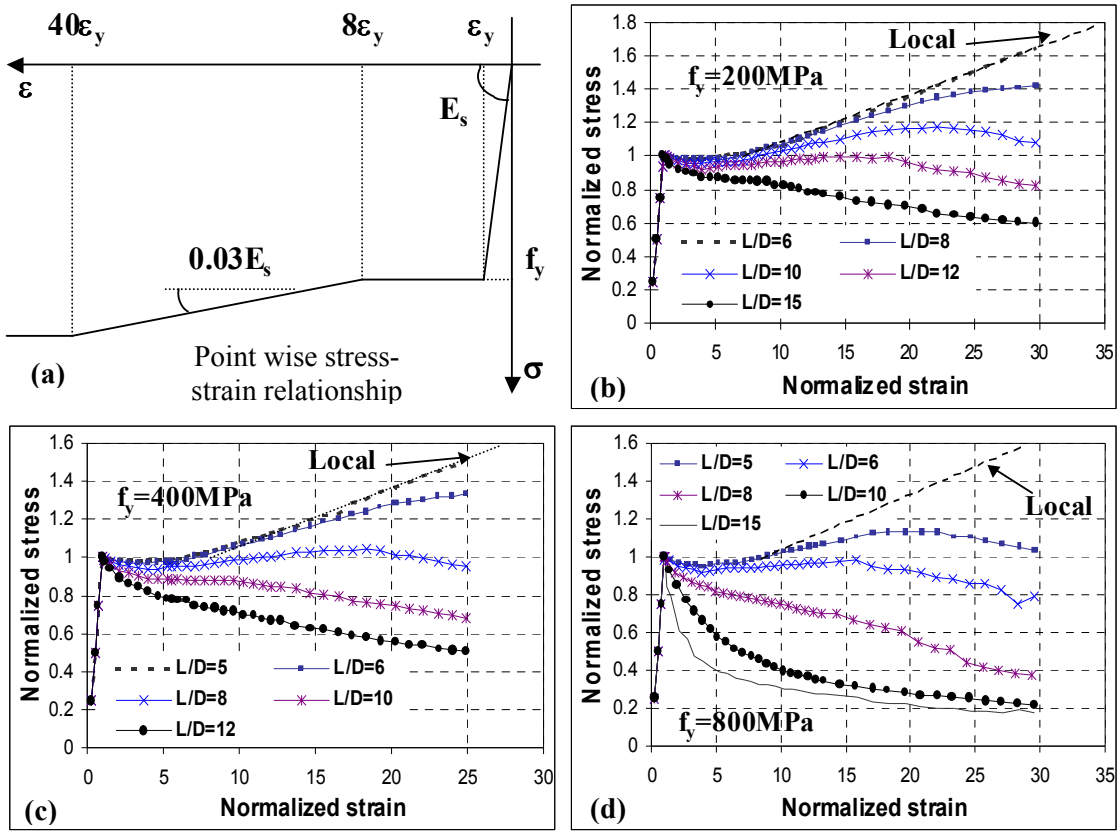
40εy
8εy
εy
ε
Es
0.03Es
fy
σ
(a)
Point wise stress-strain relationship
Local
fy=200MPa
Normalized stress
Normalized strain
L/D=6
L/D=8
L/D=10
L/D=12
L/D=15
(b)
fy=400MPa
L/D=5
(c)
L/D=5
L/D=6
L/D=8
L/D=10
L/D=15
fy=800MPa
(d)

Fig. 3

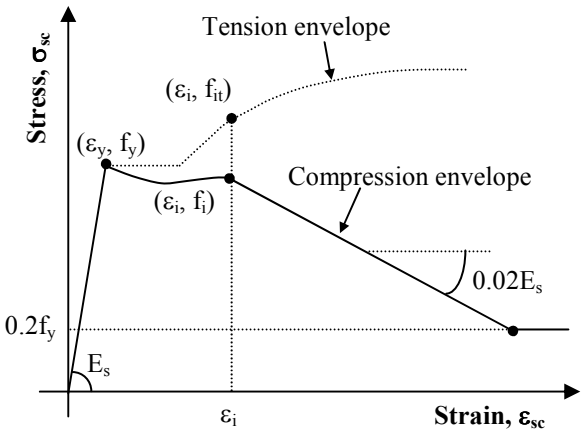
Tension envelope
Stress, σ_{sc}
(ε_i, f_{it})
(ε_y, f_y)
Compression envelope
(ε_i, f_i)
$0.02E_s$
$0.2f_y$
E_s
ε_i
Strain, ε_{sc}

Fig. 4

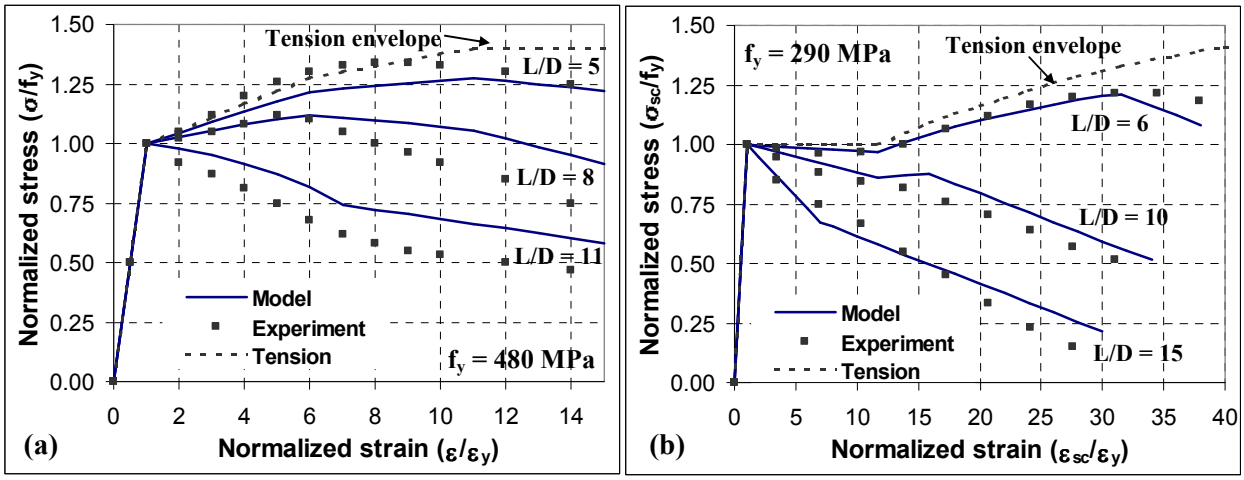
Tension envelope
L/D = 5
L/D = 8
L/D = 11
Model
Experiment
Tension
f_y = 480 MPa
Normalized stress (σ/f_y)
Normalized strain ($\varepsilon/\varepsilon_y$)
(a)
f_y = 290 MPa
Tension envelope
L/D = 6
L/D = 10
L/D = 15
Model
Experiment
Tension
Normalized stress (σ_{sc}/f_y)
Normalized strain ($\varepsilon_{sc}/\varepsilon_y$)
(b)

Fig. 5

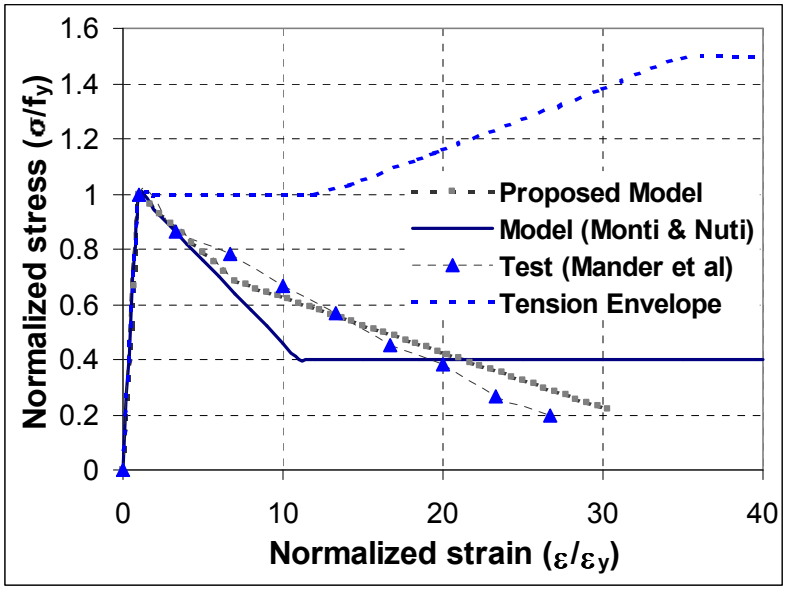
1.6
1.4
1.2
1
0.8
0.6
0.4
0.2
0
0
10
20
30
40
Normalized stress (σ/fy)
Normalized strain (ε/εy)
Proposed Model
Model (Monti & Nuti)
Test (Mander et al)
Tension Envelope

Fig. 6

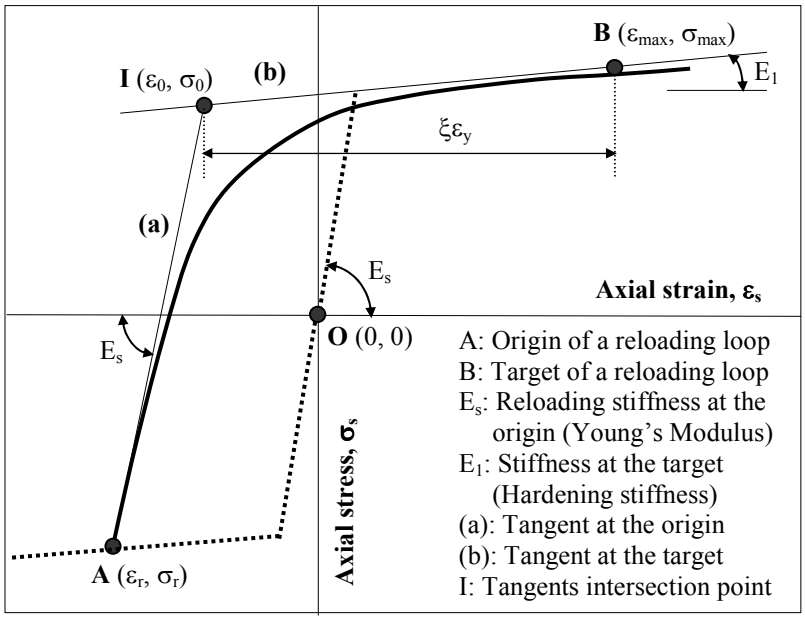
B (εmax, σmax)
I (ε0, σ0)
(b)
E1
ξεy
(a)
Es
Axial strain, εs
Es
O (0, 0)
A: Origin of a reloading loop
B: Target of a reloading loop
Es: Reloading stiffness at the origin (Young's Modulus)
E1: Stiffness at the target (Hardening stiffness)
(a): Tangent at the origin
(b): Tangent at the target
I: Tangents intersection point
Axial stress, σs
A (εr, σr)

Fig. 7

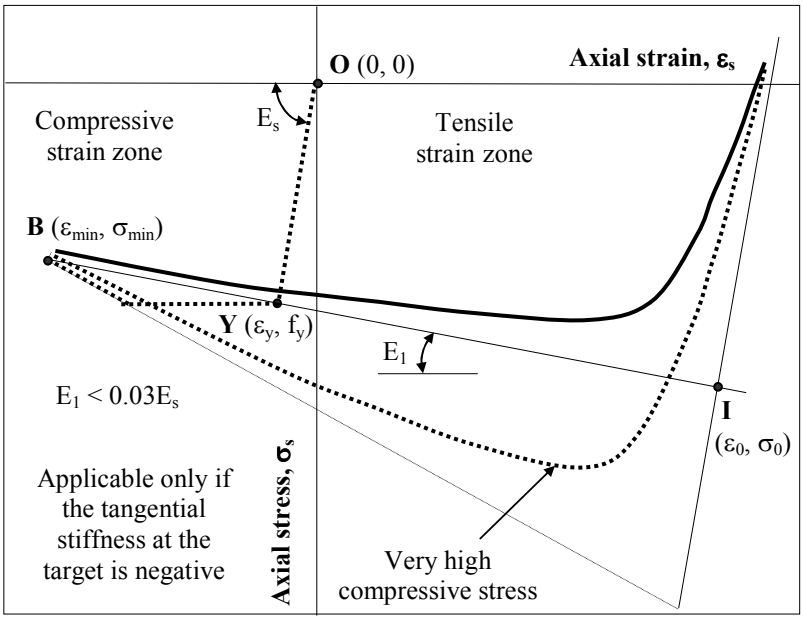
O (0, 0)
Axial strain, ε_s
Compressive strain zone
E_s
Tensile strain zone
B (ε_{min}, σ_{min})
Y (ε_y, f_y)
E_1
$E_1 < 0.03E_s$
I (ε_0, σ_0)
Applicable only if the tangential stiffness at the target is negative
Axial stress, σ_s
Very high compressive stress

Fig. 8

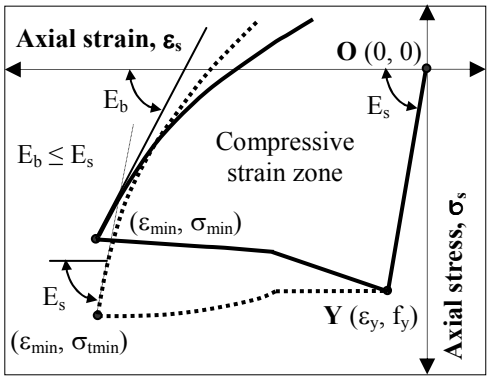
Axial strain, ε_s
O (0, 0)
E_b
E_s
$E_b \leq E_s$
Compressive strain zone
(ε_{min}, σ_{min})
E_s
Y (ε_y, f_y)
(ε_{min}, σ_{tmin})
Axial stress, σ_s

Fig. 9

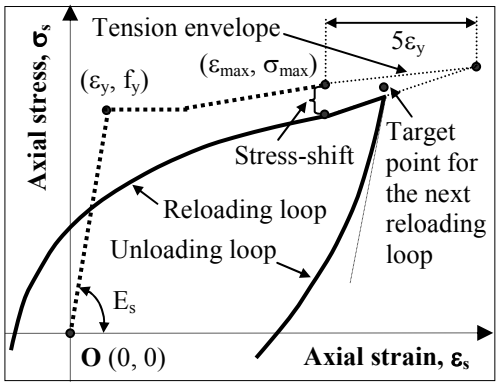
Tension envelope
$5\varepsilon_y$
$(\varepsilon_{max}, \sigma_{max})$
(ε_y, f_y)
Stress-shift
Target point for the next reloading loop
Reloading loop
Unloading loop
E_s
O (0, 0)
Axial stress, σ_s
Axial strain, ε_s

Fig. 10

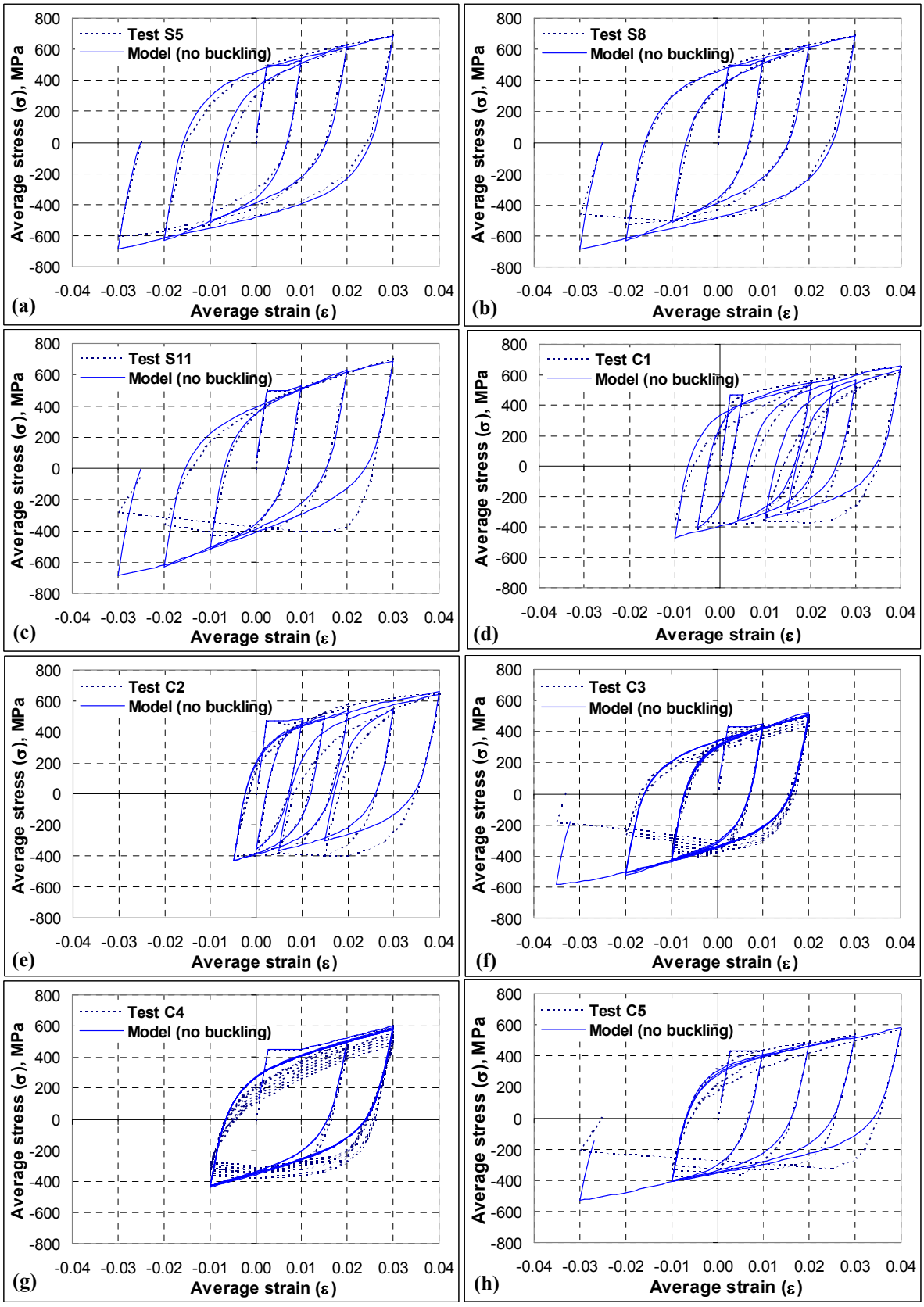
Test S5
Model (no buckling)
Average stress (σ), MPa
Average strain (ε)
(a)
Test S8
Model (no buckling)
Average stress (σ), MPa
Average strain (ε)
(b)
Test S11
Model (no buckling)
Average stress (σ), MPa
Average strain (ε)
(c)
Test C1
Model (no buckling)
Average stress (σ), MPa
Average strain (ε)
(d)
Test C2
Model (no buckling)
Average stress (σ), MPa
Average strain (ε)
(e)
Test C3
Model (no buckling)
Average stress (σ), MPa
Average strain (ε)
(f)
Test C4
Model (no buckling)
Average stress (σ), MPa
Average strain (ε)
(g)
Test C5
Model (no buckling)
Average stress (σ), MPa
Average strain (ε)
(h)

Fig. 11

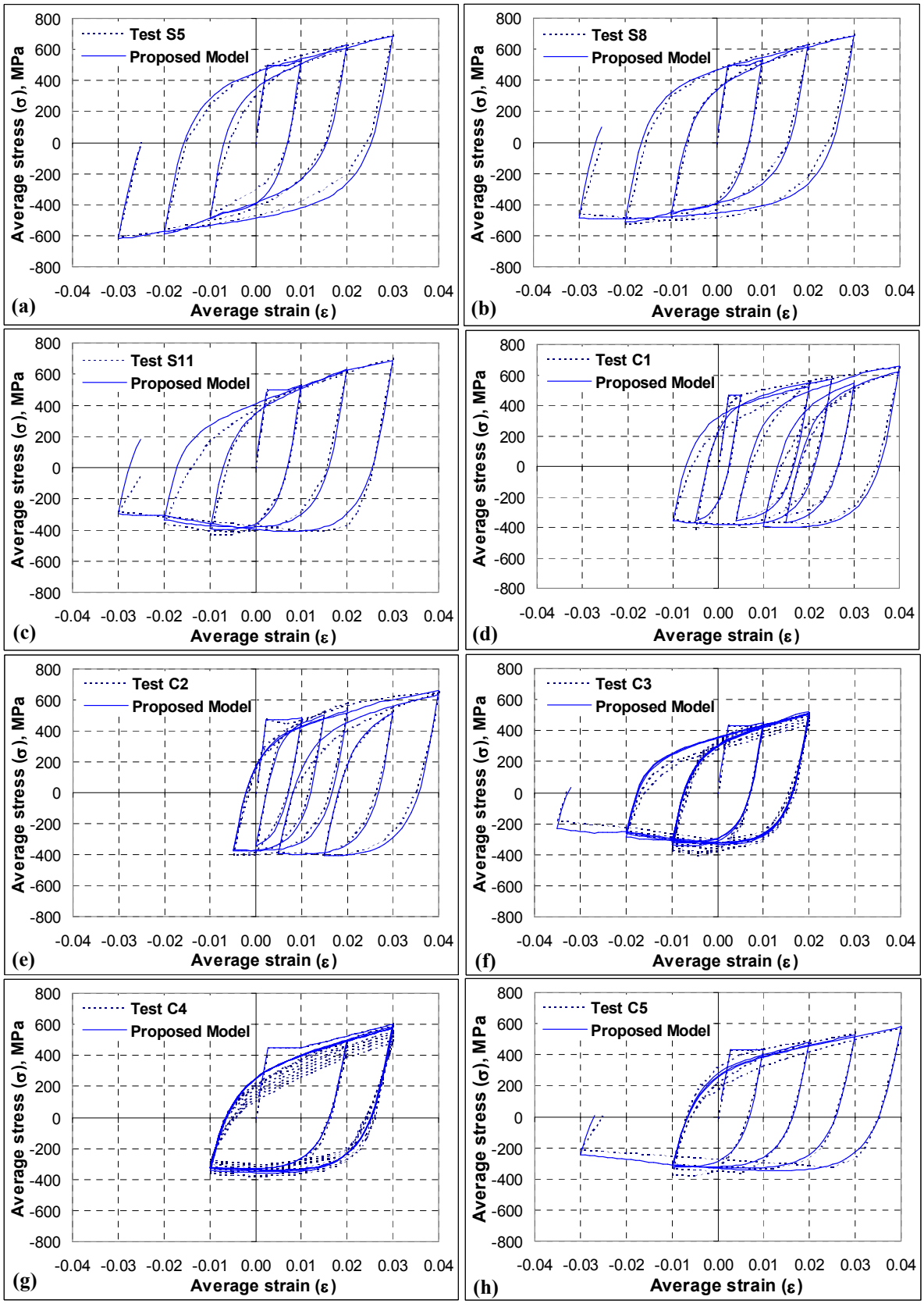
Test S5
Proposed Model
Average stress (σ), MPa
Average strain (ε)
(a)
Test S8
Proposed Model
Average stress (σ), MPa
Average strain (ε)
(b)
Test S11
Proposed Model
Average stress (σ), MPa
Average strain (ε)
(c)
Test C1
Proposed Model
Average stress (σ), MPa
Average strain (ε)
(d)
Test C2
Proposed Model
Average stress (σ), MPa
Average strain (ε)
(e)
Test C3
Proposed Model
Average stress (σ), MPa
Average strain (ε)
(f)
Test C4
Proposed Model
Average stress (σ), MPa
Average strain (ε)
(g)
Test C5
Proposed Model
Average stress (σ), MPa
Average strain (ε)
(h)

Fig. 12

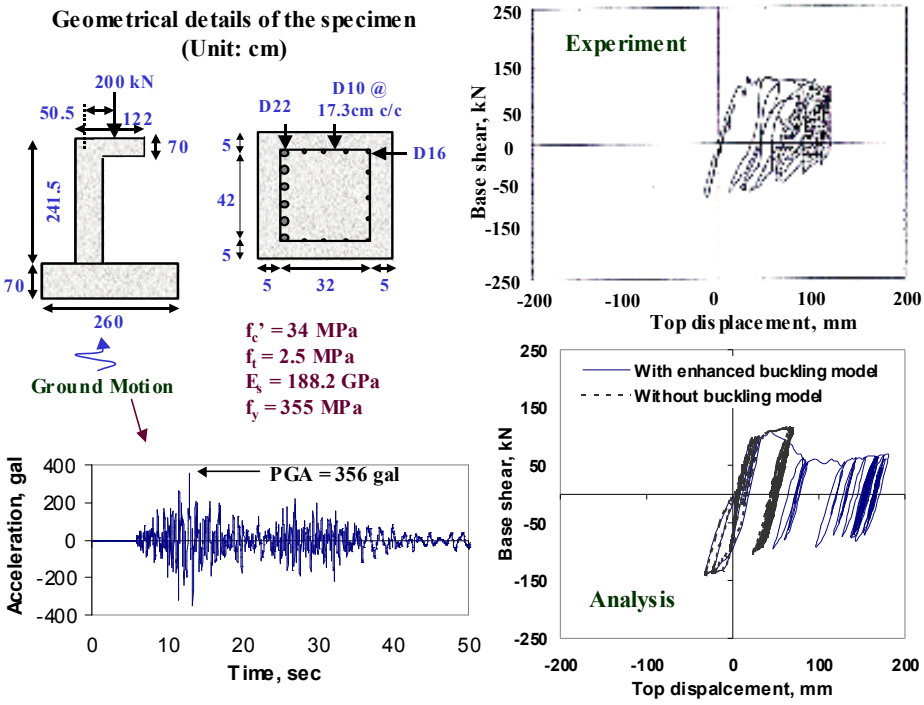
Geometrical details of the specimen
(Unit: cm)
200 kN
50.5
122
70
241.5
70
260
D22
D10 @
17.3cm c/c
D16
5
42
5
5
32
5
f_c' = 34 MPa
f_t = 2.5 MPa
E_s = 188.2 GPa
f_y = 355 MPa
Ground Motion
PGA = 356 gal
Acceleration, gal
Time, sec
Experiment
Base shear, kN
Top displacement, mm
With enhanced buckling model
Without buckling model
Analysis
Base shear, kN
Top dispalcement, mm